# Laboratory experiments on shared-energy collisions between freshwater ice blocks and a floating steel structure

Ekaterina Kim[1-3*], Martin Storheim[1-3], Jørgen Amdahl[1-3], Sveinung Løset[1], Rüdiger Ulrich Franz von Bock und Polach[3,4]

[1] *Centre for Sustainable Arctic Marine and Coastal Technology (SAMCoT), Norwegian University of Science and Technology, Trondheim, Norway*

[2] *Centre for Autonomous Marine Operations and Systems (AMOS), Norwegian University of Science and Technology, Trondheim, Norway*

[3] *Department of Marine Technology, University of Science and Technology, Trondheim, Norway*

[4] *Aalto University, School of Engineering, Espoo, Finland*

[*] Corresponding author. Email: ekaterina.kim@ntnu.no

# Laboratory experiments on shared-energy collisions between freshwater ice blocks and a floating steel structure

Ship collision with floating ice in which the ship sustains damage will be in the shared-energy regime, i.e., both the ice and the ship dissipate significant amounts of energy through inelastic deformations. The physics of such ice interactions has so far been subjected to little research. Hardly any experience exists on how to conduct shared-energy collision tests successfully. The aim of this paper is to present the concept of ice-structure collision experiments in which the impacted structure undergoes irreversible deformations together with ice failure. The paper describes laboratory-scale impact tests of freshwater ice blocks against stiffened steel panels, presents analysis of the main test results and lessons-learned. Furthermore, analytical calculations and numerical simulations were performed to support results and conclusions from the laboratory tests.

Keywords: freshwater ice; shared-energy collision; damage; laboratory experiments

## 1. Introduction

The attention towards ships operating in polar waters is increasing. Impacts with ice are the greatest cause of vessel damage in the hostile polar waters (Snider 2012). A likely outcome of a collision between a ship and an iceberg is a hull breach caused by the impact (Hill 2005). During such a collision, the deformation of the ship will change the local confinement of the ice and thereby its local stress state. This may in turn increase the crushing strength of the ice. A contribution to further knowledge on such ship-ice collisions is important for vessel design, as collision forces may rise to loads outside of the current requirements to design scenarios.

The conventional approach for the analysis of ice-structure collisions is based on the principle of energy conservation. For example, in the case of a glancing- or a head-on collision with an ice floe, the standard assumption is that the ice floe fails within the contact area in compressive crushing and the energy consumed for crushing the ice corresponds to a reduction of the combined kinetic energy of the ship and ice before and after the collision (e.g., IACS' Unified Requirements 2011 and Popov et al. 1967). In offshore engineering, this approach is usually referred to as the *strength approach* (NORSOK N-004 2013). Under these assumptions, the total force depends on the ice deformation. The local concentrations of the contact pressures are determined from the distribution of the total collision force. Several field projects were conducted in the past to measure ice pressures, loads and motions of bodies in full-scale ice impact interactions such as: the icebreaker Kigoriak test program (Varsta and Riska 1982, Ghoneim and Keinonen 1983), the icebreaker Arctic testing (German and Milne/VTT 1985 via Daley et al. 1986), the Antarctic iceberg impact experiment (Duthinh et al. 1990), the iceberg impact in Newman's Cove (Bruneau et al. 1994) and CCGS Terry Fox bergy bit trials (Ritch et al. 2008). The obtained experimental data are useful to verify parameters in the strength approach.

The so-called *ductile approach* and the *shared-energy approach* (NORSOK N-004 2013) may be used as alternative methods to assess ice-structure collisions. The ductile approach assumes that the ice feature is infinitely rigid and the dissipated energy, which is consumed by the plastically deforming ship structure, corresponds to a change of the total kinetic energy of the ship and the ice before and after the collision. The shared-energy approach assumes that both the ice and the ship structure undergo finite permanent deformations, with the instantaneously weaker structure deforming. For a ship-ice collision with significant permanent damage to the ship, the shared-energy regime is most likely. The ship will initially crush sharp local ice protrusions. As the contact area grows, the force intensity from the ice will cause inelastic deformations in the ship structure. Shared-energy analysis is challenging, because the knowledge of constitutive behaviour of both the ice and the steel is needed. The response of the ice and the structure are mutually dependent on each other.

A broad literature review (Kim and Amdahl 2013) indicates that the shared-energy approach for collisions between a floating ice-mass and a ship (or offshore structure) is not well studied compared to other two possible scenarios. Until today, only a few experimental studies of ice-structure interaction involving inelastic deformation of a structure have been performed in the field and in the laboratory. One of the first shared-energy experiments was conducted during the field test program at Hobson's Choice Ice Island in 1990 where flat indenters were pushed against an ice wedge at constant speeds. Details of the experimental setup can be found in Masterson et al. (1993). Another experiment that has been performed and published is a quasi-static laboratory test in which an ice cone was slowly pushed against a steel structure; see Manuel et al. (2013). Additionally, some experiments (e.g., those described Tuhkuri 1993) caused unexpected damage of tested structures. Many shared-energy collisions between ice masses and ships have been registered in the past (Varsta and Riska 1982 and Hill 2005). However, the available information on the extent of hull damage and the related ice characteristics that caused the damage is rather scant, and important details such as ice geometry and its strength are missing to investigate the problem in greater depth. Experimental studies on these commonly observed full-scale scenarios are thus required.

The fact that only a few experiments on shared-energy ice-structure interaction have been performed and published suggests not only a lack of attention to the shared-energy approach, but also the degree of difficulty in designing the test setups and measurement systems in order to get meaningful data. The data presented in Masterson et al. (1993) and Tuhkuri (1993) could potentially be used for validation of shared-energy ice-structure collision models, while the data in Manuel et al. (2013) lack a quantitative description of the initial parameters and the main results (geometry of the tested structure, resulting structural deformation, load-displacement curve, etc.).

The study presented in this paper is motivated by the lack of published information about testing shared-energy ice-structure collisions; considering that shared-energy is the relevant regime for a full-scale collision with damage to the ship. All the shared-energy experiments so far were performed in dry conditions at constant loading rates. This paper focuses on experimental aspects of ice-structure interactions in water, in the shared-energy regime. Experimental aspects of strength approach and ductile approach can be found elsewhere (e.g., Lindholm et al. 1990, Duthinh et al. 1990, Gagnon 2004, Gagnon 2008 and Alsos and Amdahl 2009).

This paper highlights main findings and lessons-learned from a laboratory test campaign on shared-energy collisions. It is demonstrated that under laboratory conditions, even in water, it is possible to achieve shared-energy collisions between an ice block and a floating structure.

The layout of the paper is as follows: Section 2 describes experimental setup; Sections 3 and 4 present the main test results and their analysis in which the results of numerical simulations are put in context with the experiments. Finally, a discussion and conclusions that synthesize the results of the laboratory tests and the numerical simulations are presented.

## 2. Experiment

The laboratory test campaign on shared-energy collisions was carried out to provide experience in modelling of shared-energy collisions in the laboratory conditions and to support the development of the testing procedure for a full-scale ice-structure collision scenario. The experimental focus is on the shared-energy interaction between iceberg ice (freshwater granular ice) and a stationary structure. Experimental methodology, setup and instrumentation are described in the following subsections.

### *2.1 Experimental approach*

The tests were not scaled by any similitude law. Steel-structures were used and the laboratory ice was not classic model-scale ice, but freshwater granular ice – ice of significantly higher strength. The modelling of hydrodynamic interaction was outside the scope of this study. Instead, the emphasis was placed on selecting an appropriate shared-energy collision scenario in which:

- The ice behaviour at impact should approximate behaviour of freshwater granular ice.
- The steel panel should have dimensions as to undergo permanent deformations.
- Both the ice and the structure should deform during a collision event. The ice block should be strong and have sufficient inertia to cause permanent deformations in the steel structure.

### *2.2 Test setup*

The tests were conducted in the 40 m × 40 m Aalto Ice Tank facility, which has a depth of 2.8 m. Figures 1 and 2 present a schematic and a photograph of the experimental setup.

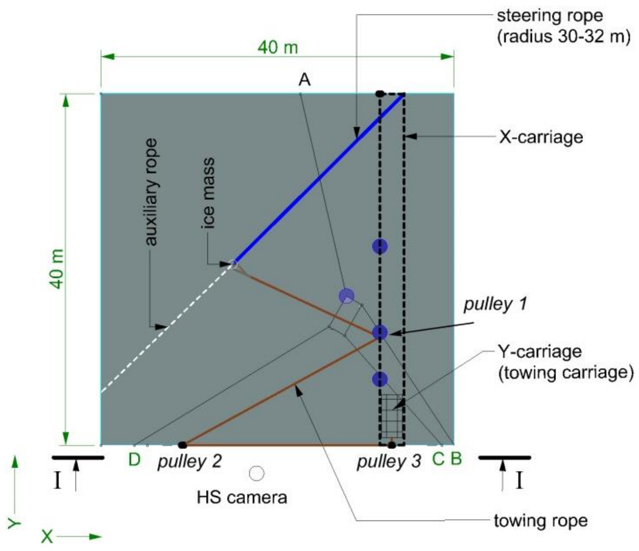


(a)

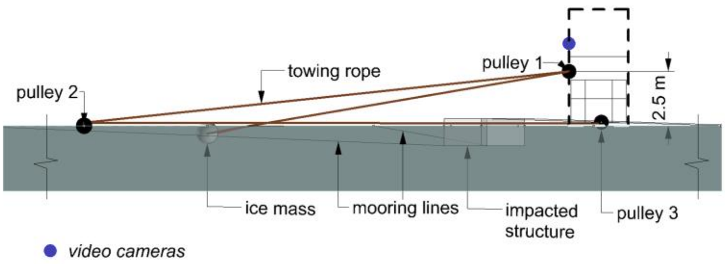


(b)

135 Figure 1. Detailed schematic of the experimental configuration: (a) plan view; the labels
136 A–D indicate mooring lines; (b) side view I-I; the slack in the mooring lines is not
137 shown in the drawings.

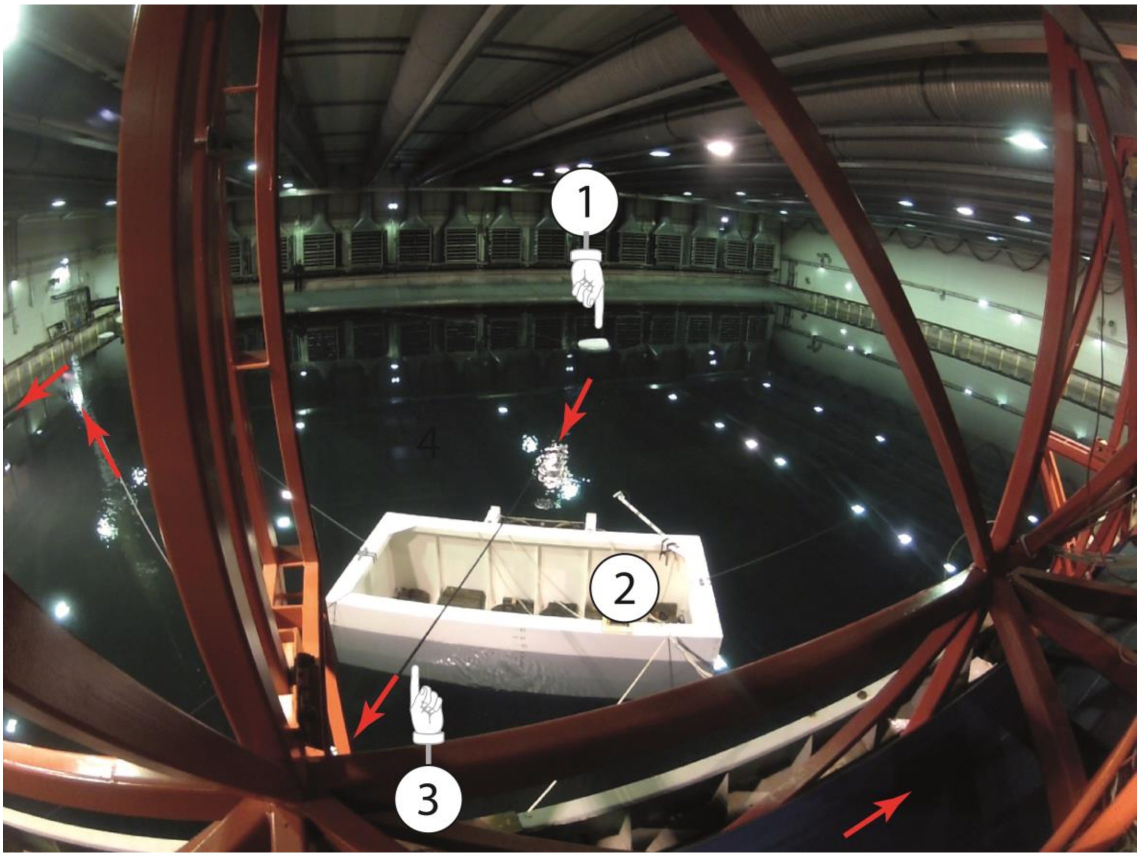


Figure 2. Photograph of the test setup: 1 – ice block, 2 – impacted target and 3 – towing rope; arrows indicate the direction of the towing arrangement; the temperature of the water in the ice tank was ~0 °C.

A system of ropes (see Figure 1) was used to tow an approximately 900-kg ice block into a purpose-built target (approximately 7.5 tons) at speeds of 1.0 and 2.0 m/s. Transverse motions of the ice block were controlled by the steering rope to obtain a direct impact on the target. An auxiliary rope (see the white rope in the plan view in Figure 1a) was used to position the ice block before each test. The ice was towed against the moored structure shown in Figure 2.

The towing test was conducted using the following procedure: the ice block was manually positioned at the desired location using the auxiliary rope. This location was selected to enable the Y-carriage (Figure 1a) to reach the desired steady-state velocity and to enable the ice block to reach the designated impact position. The ice block was controlled by a steering rope to ensure that the impact occurred near the centre of the target structure and reduce possible fishtailing motions. A V-towing scheme (Figure 3) was used to prevent the ice hook from hitting the impacted structure.

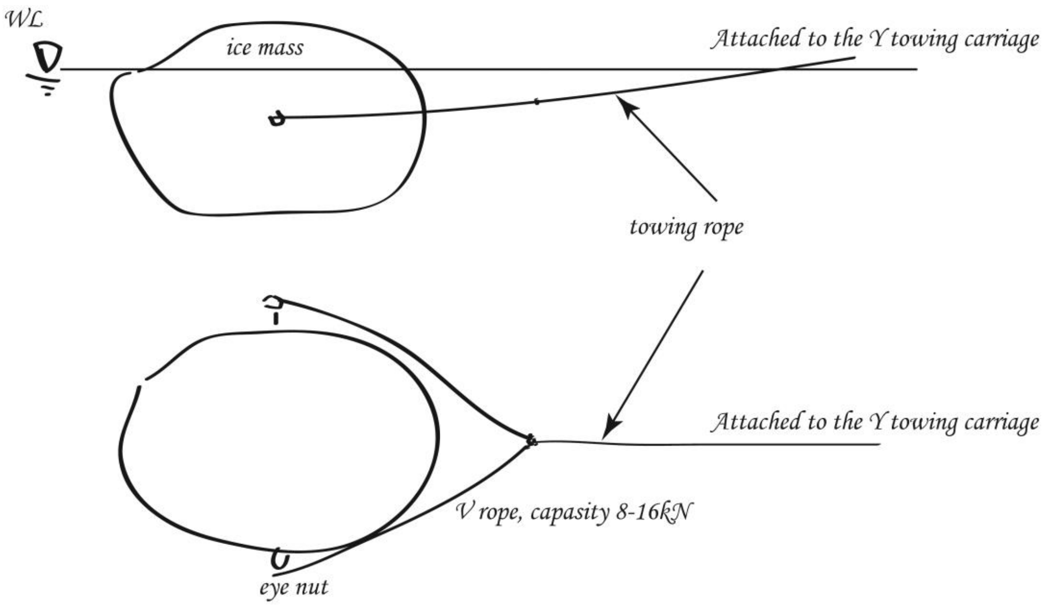


Figure 3. Side and plan view schematics of the towing arrangement.

### *2.2.1 The impacted structure*

Figure 4 shows the geometry of the impacted structure. The impacted structure, shown in Figure 4a, consisted of a stiffened panel (Figure 4b) bolted to HEB beams which were welded to a moored floater. The ballasted loading conditions for the floater with the attached 12-mm panel are listed at the top right corner in Figure 4a. The floater was moored with four 10–16 mm ø polyester mooring lines, as shown in Figure 1a. The mooring lines were attached to the bottom corners of the floater at one end and to the basin wall (a rail of the X-carriage) at the other end. All of the lines were equipped with 20-kg weights at mid-span to provide a soft mooring response with low forces until there was significant sway and surge displacement of the floater. Thus, the soft mooring arrangement did not affect the measured impact loads or velocities, but motions of the floater after impact.

Four steel panels of different configuration were used to simulate the desired interaction between the ice block and the structure. The test panels were not scale models of any particular ship structure, but a representative panel that could behave similar to a ship structure at the given experimental scale (more below). Figure 4c presents a plan view of the impacted panel, highlighting the different structural elements of the panel. The dimensions of the structural elements (i.e., plate thickness, stiffener spacing and frame spacing) are based on the following considerations:

- The ice pressure is uniformly distributed over the $s \times s$ loading patch ($s$ denotes the stiffener spacing).
- The experimental data obtained for freshwater ice indentation at medium- and small scale is used for estimation of the ice pressure within the $s \times s$ contact area.
- The plate-strip analogy is used to predict onset of irreversible deformations.
- Three different numerical methods are used to predict structural deformations during the collision event. These include a simplified nonlinear static analysis, quasi-static (displacement control) analysis and dynamic (velocity controlled analysis). For details refer to Kim et al. (2012b).

The overall dimensions of the panel were 1.1×1.3 m. The panel was supported by six transverse flat-bar stiffeners and by two longitudinal flat-bar frames as shown in Figures 4b and 4c. Table 1 lists the panel parameters.

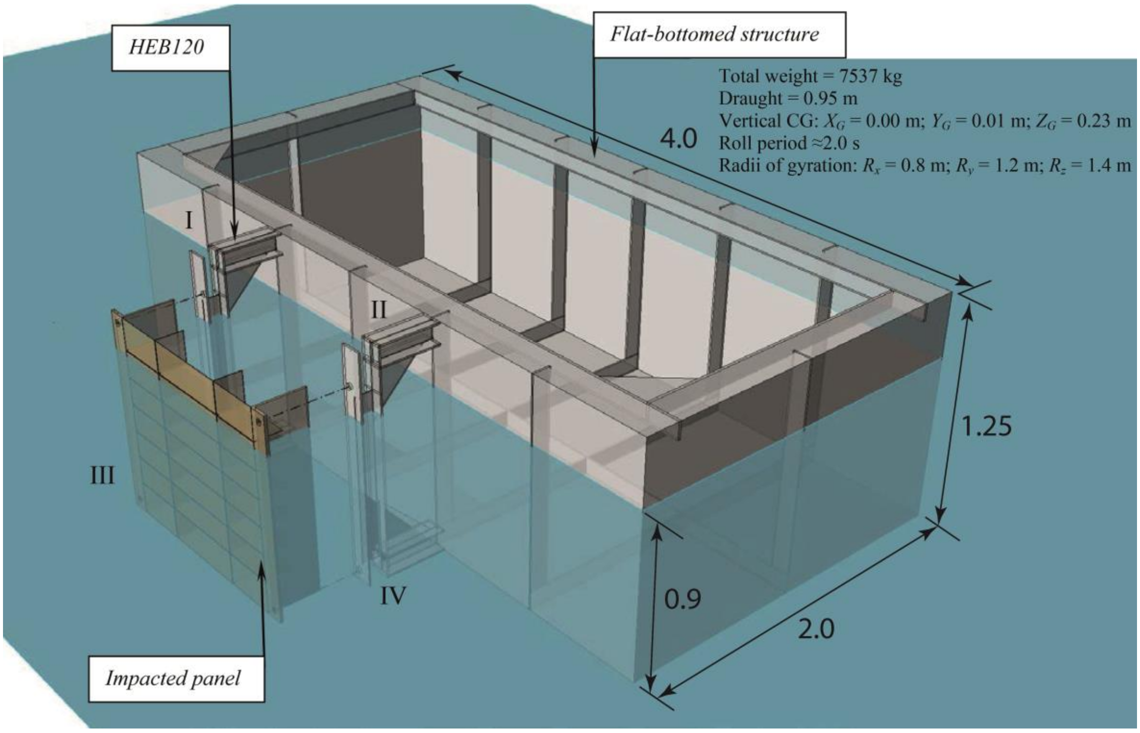
HEB120
Flat-bottomed structure
Total weight = 7537 kg
Draught = 0.95 m
Vertical CG: $X_G$ = 0.00 m; $Y_G$ = 0.01 m; $Z_G$ = 0.23 m
Roll period ≈2.0 s
Radii of gyration: $R_x$ = 0.8 m; $R_y$ = 1.2 m; $R_z$ = 1.4 m
4.0
I
II
III
IV
1.25
0.9
2.0
Impacted panel

(a)

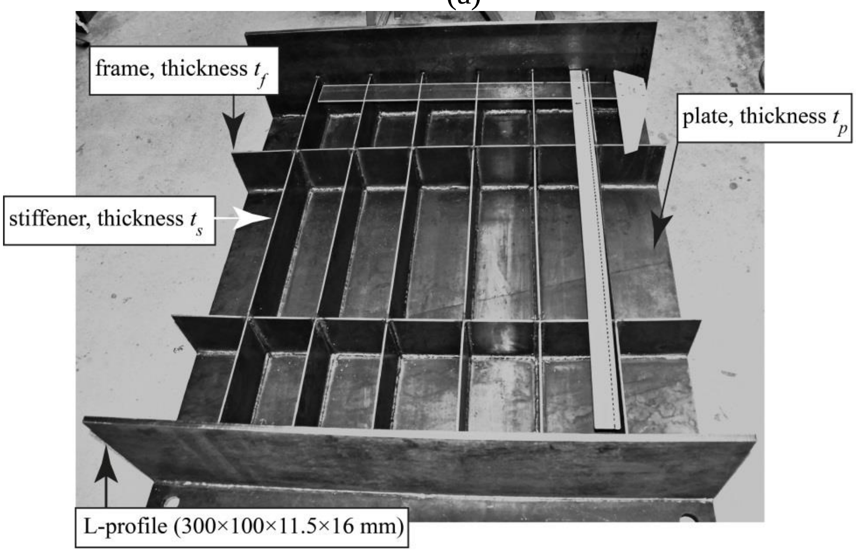
frame, thickness $t_f$
plate, thickness $t_p$
stiffener, thickness $t_s$
L-profile (300×100×11.5×16 mm)

(b)

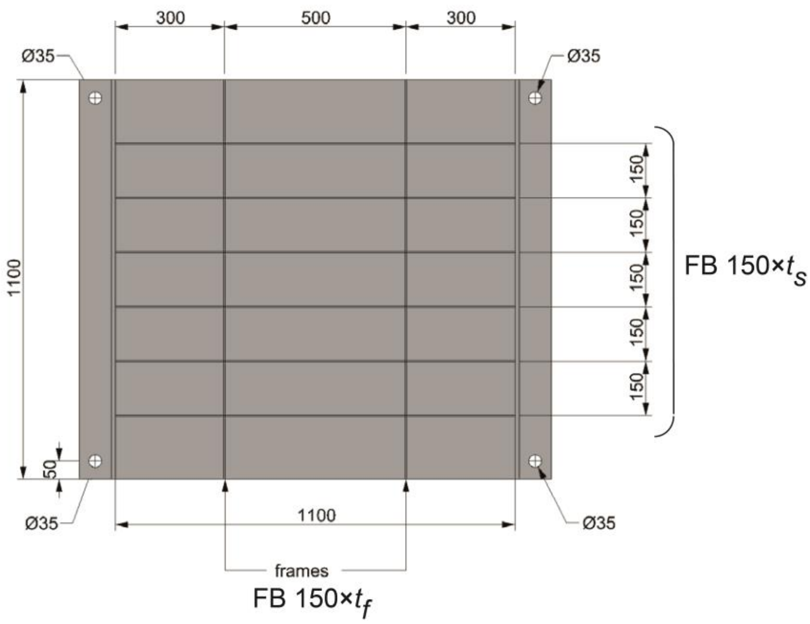


(c)

Figure 4. Geometry of the impacted structure: (a) attachment scheme of a stiffened panel with the floater, dimensions are in meters; (the floater ballast conditions include panel D); (b) photograph of a stiffened panel showing the main structural components; and (c) detailed drawing of the impacted panel (all dimensions are in millimetres).

Table 1. Test panel dimensions and material strength.

| Panel | Material | Thickness, $t_p$–$t_s$–$t_f$ (mm) | Mass (kg) | Measured engineering yield stress of the plate (MPa) |
|---|---|---|---|---|
| A[a] | Mild steel S235 | 4–2–4 | 155 | 300[c] |
| B[a,b] | Mild steel S235 | 2–2–2 | 131 | 190 |
| C[b] | Mild steel S235 | 4–4–4 | 171 | 300[c] |
| D[a] | Mild steel S235 | 12–12–12 | 330 | Not measured |

[a] Used in impact tests in water; [b] Used in drop tests; [c] Experiments reveal a yield peak of 360 MPa (stress – strain curves can be found in Kim et al. 2013).

### *2.2.2 The ice*

Iceberg ice has a predominant granular structure and low or no salinity. To mimic these, the ice blocks were manufactured in plastic containers with in-plane dimensions of 1.0×1.2 m and a height of 0.9 m. The containers were filled up with crushed ice and water. To facilitate specimen handling, a threaded metal rod was frozen into the ice. The threaded rod, with eye nuts attached to both ends, provided connection points for the system of ropes that was used during lifting and towing of ice. A total of 10 containers were filled and packed with commercially available crushed ice. The crushed ice was ordered from a third-party company and had a piece size of approximately 10–40 mm (Figure 5a). Subsequently, water was added from the bottom to avoid air entrapment. The containers, filled with the mixture of water and crushed ice (Figure 5b), were stored at –20 °C to freeze completely. The freezing process was monitored by two temperature sensors in the ice at depths of approximately 0.4 m and 0.1 m. Furthermore, the freezing process was accelerated, and the internal stresses in the ice (due to multiaxial freezing) were decreased by drilling holes, approximately 0.3 m deep, into the ice near the threaded bar. These holes enabled unfrozen water to flow to the surface of the block, releasing some of the internal pressure.

The ice blocks were considered to be frozen once the temperature at both sensors attained the ambient temperature of –20 °C. It took approximately 5 days to completely freeze the samples. In case visible cracks formed during the freezing process, those were sealed with fresh water earlier than 24h prior to testing.

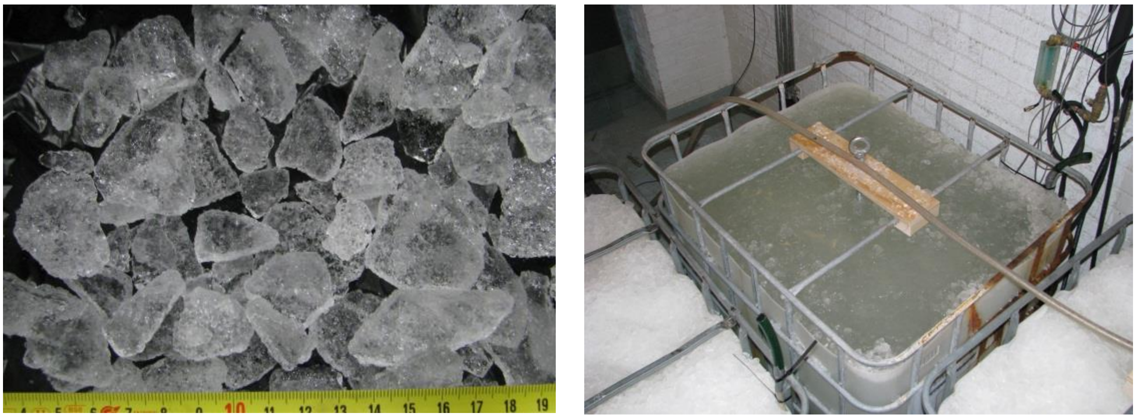

(a) (b)

Figure 5. (a) –A photograph of crushed ice pieces used to fill the containers. On the ruler, longer lines with numbers are in centimetres and shorter lines are in millimetres; (b) – a photograph of a container filled with mixture of crushed ice and water.

Prior to testing, the ice block was examined for signs of open cracks and unfrozen water pockets. In case of detecting long cracks which might endanger integrity of the ice block, the block was not used. Solid ice blocks were cut into the final test shape (a truncated prism). Figure 6 presents idealized geometry and a photograph of a typical ice block used in the impact tests.

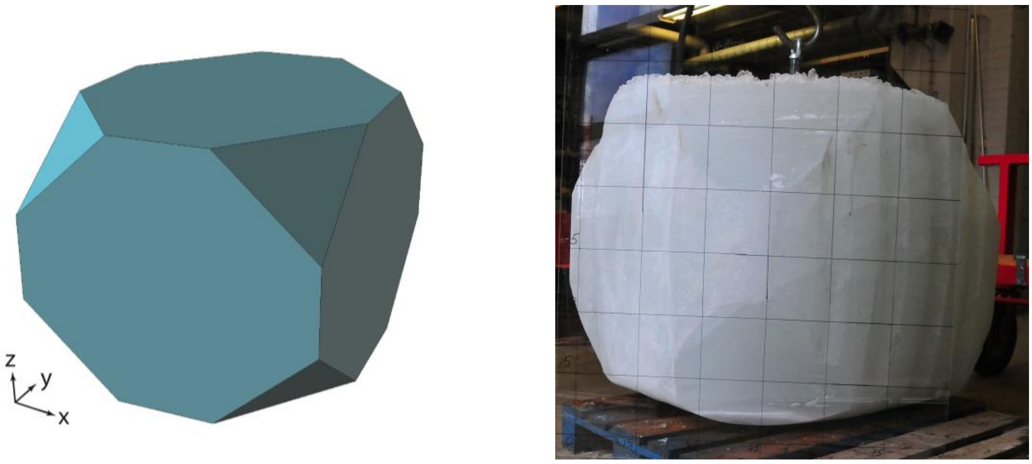


(a) (b)

Figure 6. Final shape of the ice block: (a) – idealized geometry; (b) – a photograph of a typical ice block (the grid lines are 0.15 m apart). The final shape of the ice was formed

by cutting out eight approximately equal-sized tetrahedrons from the corners of the prismatic ice block (~1.0×1.1×0.9 m).

*Compressive strength under uniaxial loading*

To demonstrate the behaviour of the laboratory-grown freshwater ice compared to other published data, uniaxial compressive tests were performed with specimens extracted from the manufactured ice blocks. Each specimen was cut to a prismatic shape of the desired size (approximately 5×5×15 cm). Each ice sample was weighed and measured before testing to assess the ice density. The testing was performed at an ambient temperature of 0 °C and at a loading speed of approximately 17 mm/s. Figure 7 shows a typical force-time history and a contact pressure distribution at the time of the maximum force.

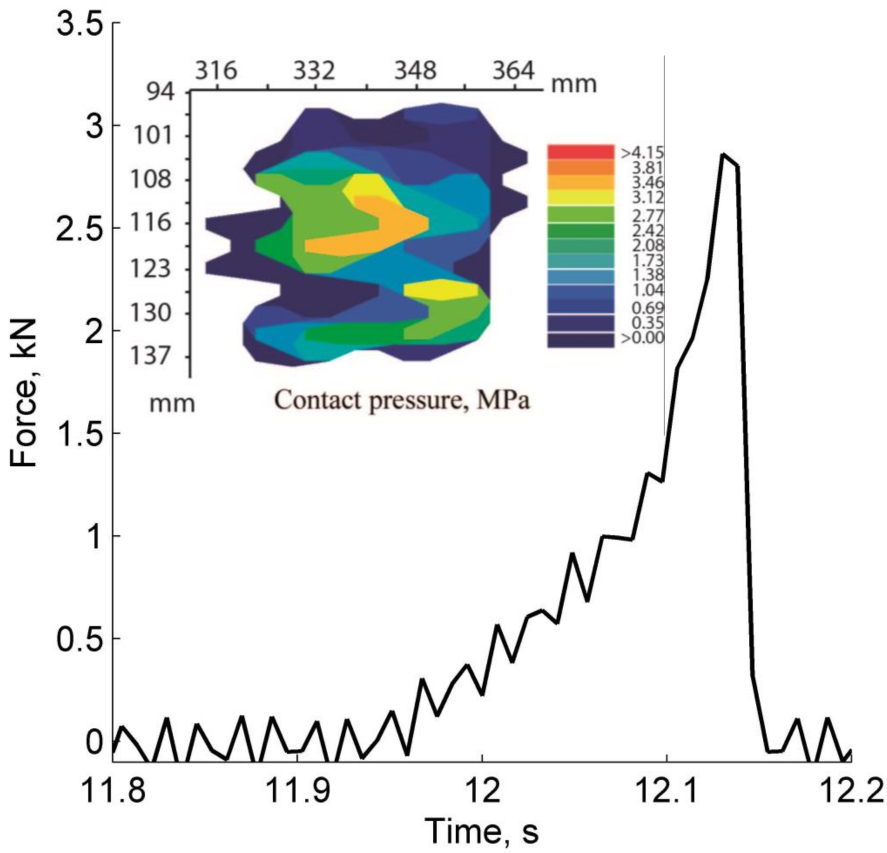

Figure 7. A force-time signal that was recorded during a uniaxial compressive test on ice (Block F); the contact pressure distribution was measured by a tactile pressure sensor at the time of the maximum force.

The ice samples exhibited a density of 901±11 kg/m$^3$ (indicating an average porosity of approximately 2%) and a compressive strength of 0.80±0.10 MPa in brittle-like failure mode under uniaxial loading conditions. The brittle-like failure mode was characterized by a sharp decrease of the load after ice failure.

*Microstructure of ice*

To examine undamaged ice microstructure, thin sections were produced from the manufactured ice blocks. The pieces were collected from both virgin ice and ice that was tempered in the ice basin (block C). These pieces were stored at –10 °C before their microstructure was examined. Thin sections of all of the ice samples were obtained using the technique described in Kim et al. (2012a). Figures 8a and 8b show close-up photographs of the manufactured ice.

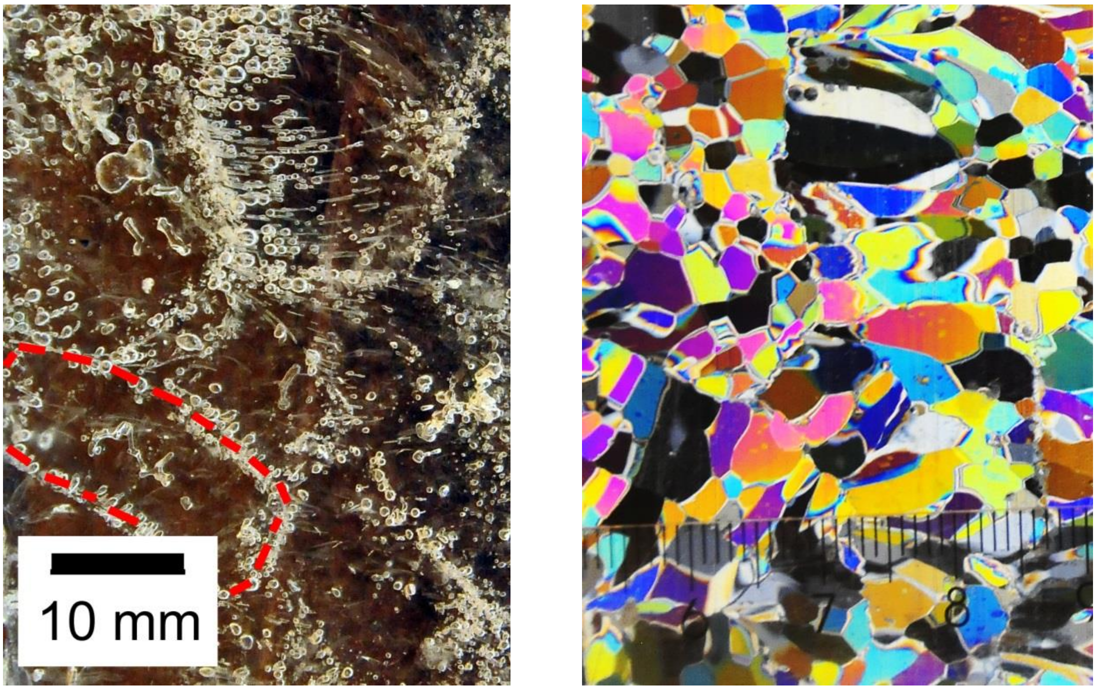


(a) (b)

Figure 8. Photographs of the laboratory-grown ice: (a) an example of air entrapped in the manufactured ice; the dashed line indicates ice-piece boundaries with entrapped air; (b) heterogeneity in the grain size of manufactured ice (a thin section of ice photographed under cross-polarized light); the scale at the bottom is in millimetres.

The internal structure of the ice specimens did not exhibit large variations in texture, except for the top most layer of the ice block (not shown in Figure 8). The manufactured ice was relatively homogeneous in all of the thin sections, with grain sizes varying between 2 mm and 10 mm. Air bubbles with diameters of 1 mm or less were mainly found (see Figure 8a) along the boundaries of the ice pieces which were used to manufacture ice blocks.

### ***2.3 Instrumentation***

Each impact event was recorded from five different angles using a high-speed FASTCAM-APX video camera and four GoPro HD Hero 2 video cameras, which were mounted as shown in Figure 1. Additionally, a video camera was mounted on the upper right side of the floating structure to record an oblique angle view of the impact zone and to provide additional information about the eccentricity of the impact and the orientation of the ice block prior to impact. The high-speed video camera was mounted on the side of the ice basin and recorded images at 500 frames per second.

The impact force transferred through each of the four HEB beams (denoted I–IV in Figure 4a) was measured by three uniaxial strain gages, which were attached along the beam flange, across the beam flange and at an angle of 45° to the beam web neutral axis.

A dynamic motion unit recorded accelerations and the angular rates of the floater and the attached stiffened panel. The strains, accelerations and angular rates were recorded using a data acquisition system at a sampling frequency of 523 Hz, which was the highest sampling frequency possible with this equipment. This system ensured that the strain and acceleration measurements were synchronized.

In addition to the towing tests described, two drop tests in dry conditions were conducted. A detailed description of the drop tests can be found in Kim et al. (2013). These tests characterize the ice-stiffened panel interaction in the absence of hydrodynamic effects. In Drop Test no. 1, a 706-kg ice block is dropped onto B panel from a height of 0.5 m, and in Drop Test no. 2, a 601-kg ice block, is dropped onto C panel from a height of 3.0 m. In Drop Test no. 1, the kinetic energy and the global shape of the ice block before impact are similar to those for the impact tests in water at 2.0 m/s. The kinetic energy was approximately 3.5 kJ in Drop Test no. 1 and approximately 2.7 kJ and 2.6 kJ for impact Test nos. 8 and 9. An added mass coefficient of 0.5 was used in calculations of the kinetic energy before impact in water and is in agreement with the values reported in Bass and Sen (1986).

The plate deflection profiles were manually recorded before and after each test. Readings of the surface profiles were done on a flat, vibration-free surface by using a plunger-type dial gage. Final deformations of A–C panels were computed as the difference between the measured plate deflections before and after the impact.

## 3. Laboratory tests results

A total of 18 impact tests were conducted in water. Of these, 16 impacts were conducted using the 12-mm-thick panel (D panel) to determine whether reproducible results could be obtained with the experimental configuration. There was a significant scatter in impact location. Repetitions of a single test revealed difficulties in ensuring the exact impact conditions for each test, e.g., with respect to the horizontal impact location on the panel. From 18 tests, only the four most interesting runs will be presented in this paper. These are the tests within the shared-energy regime in which both the ice and the structure underwent crushing or permanent deformations (Test nos. 8 and 9) and the most central impacts in which the structure remained intact (Test nos. 4 and 11). Table 2 presents the parameters for the representative tests and the corresponding ice properties. It lists type of the impacted panel, initial ice velocity, mass of the striking ice, compressive strength of the ice under uniaxial loading and the density. The table also indicates whether the weak links were broken during the impact. The tabulated values of the initial ice velocity correspond to the speed of the Y- towing carriage immediately before the impact. Significant data measured/estimated in the impact tests are listed in Table 3 and are followed by the information on how these data were obtained. Table 4 lists a summary of the drop tests.

Table 2. List of parameters and ice properties during impact tests in water.

| Date 2012 | Test no. | Panel | Velocity ($m\ s^{-1}$) | Ice mass (kg) | $\sigma_C$ (MPa) | Ice density ($kg\ m^{-3}$) | Weak link |
|---|---|---|---|---|---|---|---|
| 30/03 | 4 | D | 1 | C = 920 [b] | 0.77 ± 0.16 [i] | 914 ± 15 [i] | No |
| 02/04 | 8 | B | 2 | E = 897 | 0.71 ± 0.18 [j] | 894 ± 7 [j] | Yes, 16 kN |
| 03/04 | 9 | A | 2 | F = 850 | 0.91 ± 0.29 [k,a] | 896 ± 9 [k,a] | Yes, 5 kN |
| 04/04 | 11 | D | 2 | F [l] | 0.91 ± 0.29 [k] | 896 ± 9 [k] | Yes, 5 kN |

[i, j, k] number of tested ice samples (i=5, j=6, k=7)

[l] sample was in water over night

[a] measured one day after the test

[b] measured one day before the test

Table 3. Summary of partial test results.

| Test no. | Maximum panel deflection (mm) | Peak load [b*] (kN) | Loads via HEB beams [a], % I | II | III | IV | Impact duration [a(b)] (ms) | Velocity before impact [c(d)] ($m\ s^{-1}$) | Common velocity after impact [f(e)] ($m\ s^{-1}$) | Maximum sway acceleration (floater) ($m\ s^{-2}$) |
|---|---|---|---|---|---|---|---|---|---|---|
| 4 | – | 146 | 37 | 45 | 8 | 10 | 29 (33) | 0.9 (0.0) | 0.22 (0.13) | 13.8 |
| 8 [cr] | ≈5 | 190 | 18 | 17 | 33 | 31 | 36 (31) | 1.5 (0.0) | 0.40 (0.31) | 18.5 |
| 9 [s] | ≈3 | 226 | 31 | 28 | 19 | 22 | 35 (36) | 1.5 (0.1) | 0.29 (0.44) | 21.9 |
| 11 | – | 222 | 15 | 28 | 23 | 33 | 27 (21) | 1.8 (0.1) | 0.20 (0.24) | 21.0 |

[a] Unfiltered data from strain gages at 45°, expressed in terms of % distribution of the force in each beam.

[b*] Unfiltered data from DMU, $F = (M_s + 0.4M_s)a_s$, $a_s$ is the maximum sway acceleration of the floater.

[b] Estimated from the measured acceleration data integrated over time.

[c] Averaged ice-block velocity from high speed video records.

[d] Averaged velocity of the floater estimated from high speed video recording.

[e] Velocity after impact, as estimated from the acceleration data.

[f] Velocity of the floater after impact, as estimated from high speed video records.

[cr,s] crushing- and splitting-dominated ice failure, respectively

Table 4. List of parameters during drop tests in dry conditions.

| Date 2012 | Test no. | Panel | Drop height (m) | Ice mass (kg) | Kinetic energy (kJ) | Max. length of dent (mm) | Max. depth of dent (mm) |
|---|---|---|---|---|---|---|---|
| 30/03 | 1 [cr] | B | 0.5 | 706 | 3.5 | 600 | 13 |
| 30/03 | 2 [s] | C | 3 | 601 | 17.7 | 750 | 8 |

[cr,s] crushing- and splitting-dominated ice failure, respectively

### *3.1 Permanent plate deformations*

In all of the cases using the 12-mm panel (D panel), the structure was sufficiently strong to crush the ice with no permanent deformation on the impacted plate. The weaker panels sustained damage. Figure 9 shows the measured plate deflections after impact Test nos. 8 and 9. For the purpose of comparison, the measured plate deflections after the drop tests are provided in Figure 10a and Figure 10b. The black horizontal and vertical lines indicate the locations of the stiffeners and the frames.

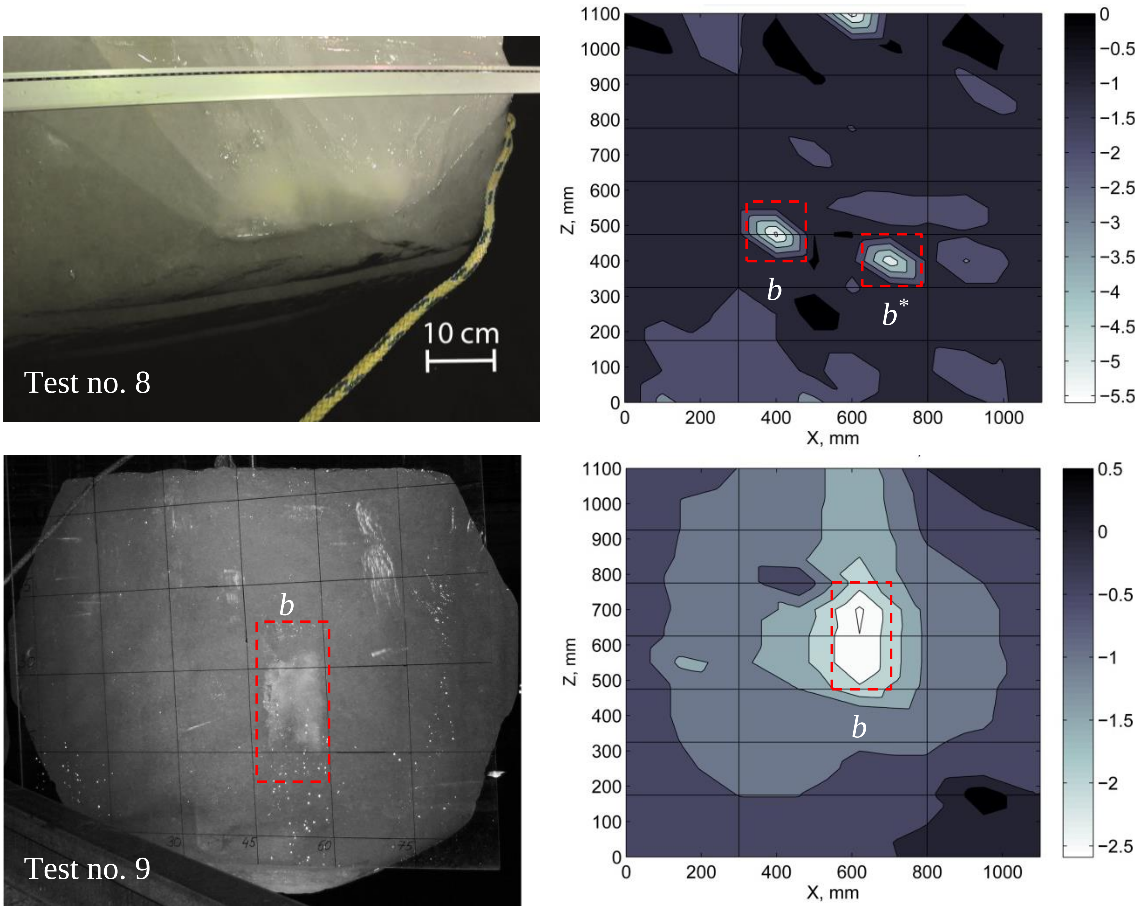


Figure 9: Photographs showing the ice damage zone after Test nos. 8 and 9 (for a grid size of 0.15 m) and the resulting deflections of the 2-mm plate in Test no. 8 and the 4-mm plate in Test no. 9; the deflections are given in mm; the assumed load patch is shown by the dashed lines, *b* is the width of the assumed load patch ($b$=$b^*$= 0.15 m).

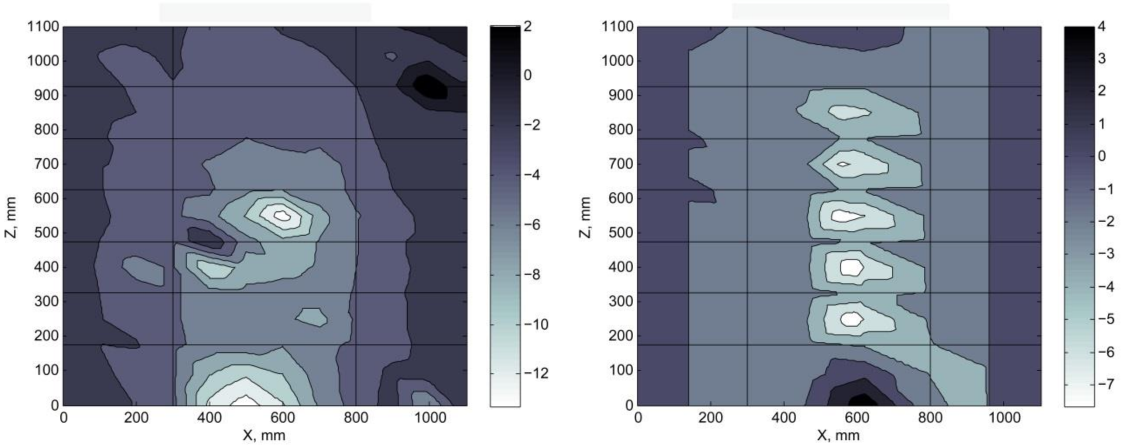


(a) (b)

Figure 10: Plate deflections after the drop tests, deflections are given in millimetres (mm): (a) – Drop Test no.1 (B panel) and (b) – Drop Test no. 2 (C panel).

Figure 11 is a photograph of the plate damage resulting from the drop test from a height of 3.0 m (Drop Test no. 2).

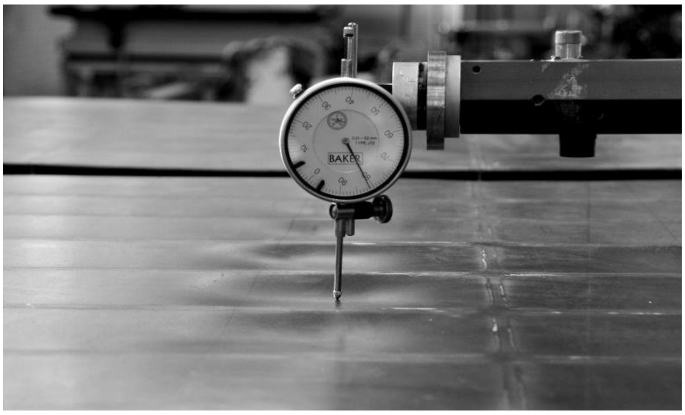


Figure 11. A photograph of the plate damage after Drop Test no. 2 (Kim et al. 2013).

### *3.2 Ice damage*

The ice behaviour was governed either by localized crushing or by splitting. This classification was made through visual observations of ice blocks upon impact. During crushing, the ice block remained intact except for the crushed region; the ice crushing was localized specifically at the contact zone. The splitting-dominated failure resulted in complete shattering of the ice block upon impact. The ice crushing failure dominated in the impact tests in water (Test nos. 8 and 9) and in Drop Test no. 1. The splitting failure dominated in Drop Test no. 2, i.e., the test with the largest kinetic energy of ice before impact. The observed ice failure is indicated in Tables 3 and 4. Figure 12a and Figure 12b are close-up photographs of ice damage after Drop Test no. 2 and Test no.8, respectively.

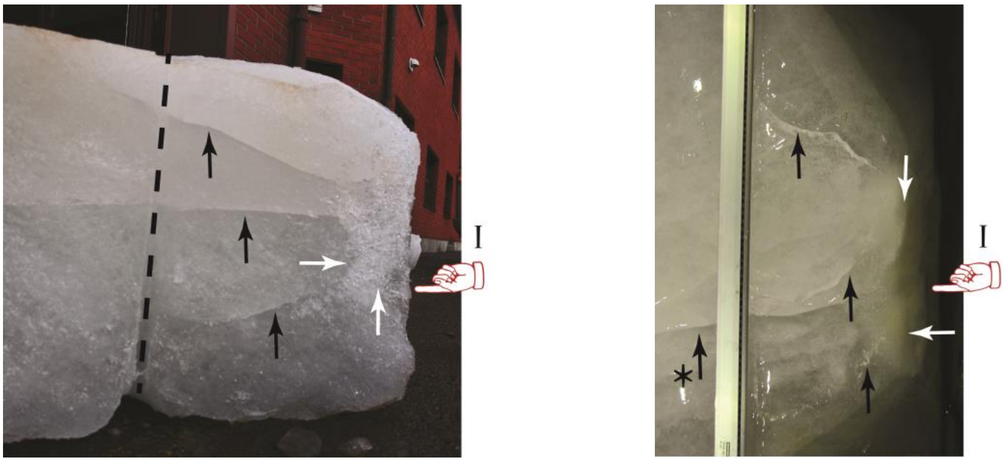


(a) (b)

Figure 12: Photographs of ice damage: (a) – a portion of the ice block after Drop Test no. 2; (b) – a close-up view after Test no. 8. Black arrows indicate freshly-formed splitting cracks, and white arrows indicate crushed ice. The arrow with a star indicates an ‘old’ crack (i.e., the crack that was healed using freshwater before the freezing process of the ice block was completed). The dashed line indicates the position of the metal rod, which was frozen into the ice to facilitate specimen handling. A hand symbol with label ‘I’ indicates the direction of impact.

### *3.3 Impact force*

The impact force was derived from the measured accelerations of the floater (DMU) and from strain gages (SG). The total force ($F_{sg}$) from beams I–IV (Figure 4) was calculated using unfiltered measurements from the 45° oriented strain gages and represented the panel response to the impact (Equation 1).

$$F_{sg}(t) = \sum_{1}^{4} F(t)_i = E_{steel} A_{HEB} \cos(45) \sum_{1}^{4} e_i(t) \quad (1)$$

$F_i(t)$ is the load history for each HEB beam; $E_{steel}$ is the elastic modulus of steel; $A_{HEB}$ is the cross-section area of each HEB beam (34 cm$^2$); $e_i$ is the recorded strain-time history at location *i*. The distribution of the maximum total load via the beams I–IV (expressed as a percentage) is reported in Table 3 (in the column "Loads via HEB beams").

The peak impact load for each run ($F_p$, see the column "Peak load" in Table 3) was estimated from the measured sway acceleration of the floater as $F_p=(M_s+A_s)a_s$, where $M_s$ is the total mass of the impacted structure, $a_s$ is the maximum acceleration of the floater in Table 3 and $A_s$ is the hydrodynamic added mass of the structure in the sway direction. $A_s=0.4M_s$ was assumed (Petersen and Pedersen 1981). Figure 13 presents the impact force histories for Test no. 8 and 9.

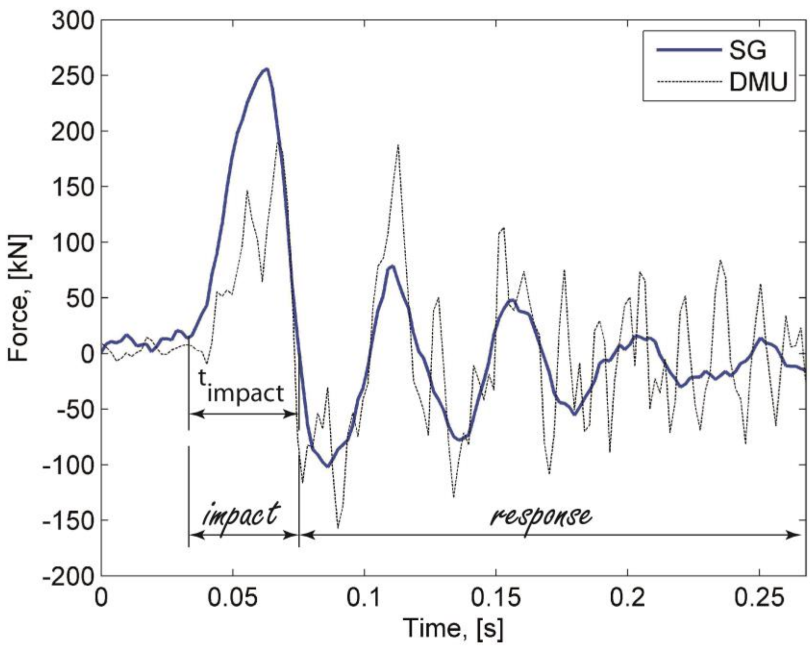

(a)

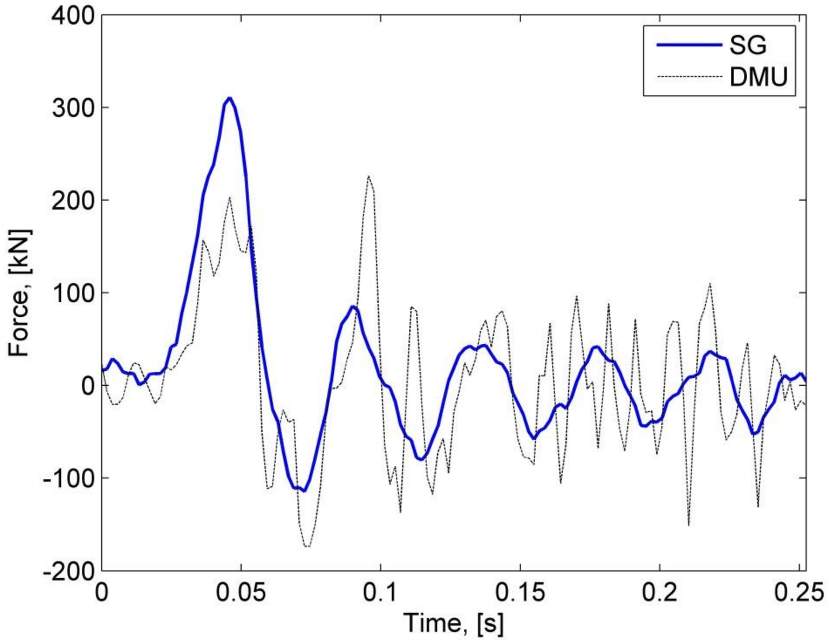


(b)

Figure 13: Impact force versus time: (a) – for the collision interaction between the 897-kg ice block and B panel (Test no. 8); (b) – for the collision interaction between the 850-kg ice block and A panel (Test no. 9); the strain-gage-measurement based impact force (SG) was estimated from the 45° oriented strain gages; the dynamic-motion-unit measurement based impact force (DMU) was estimated from accelerations of the floater in the sway direction; note that the reported SG and DMU forces are normal to the floater side surface.

### *3.4 Impact duration and impact velocity*

In order to determine the impact duration, the data from strain gages and the dynamic motion unit (DMU) were used. The duration of the impacts is listed in Table 3. Figure 13a and Figure 14 illustrate how the impact duration ($t_{impact}$) was determined from the strain gage data and the DMU data, respectively.

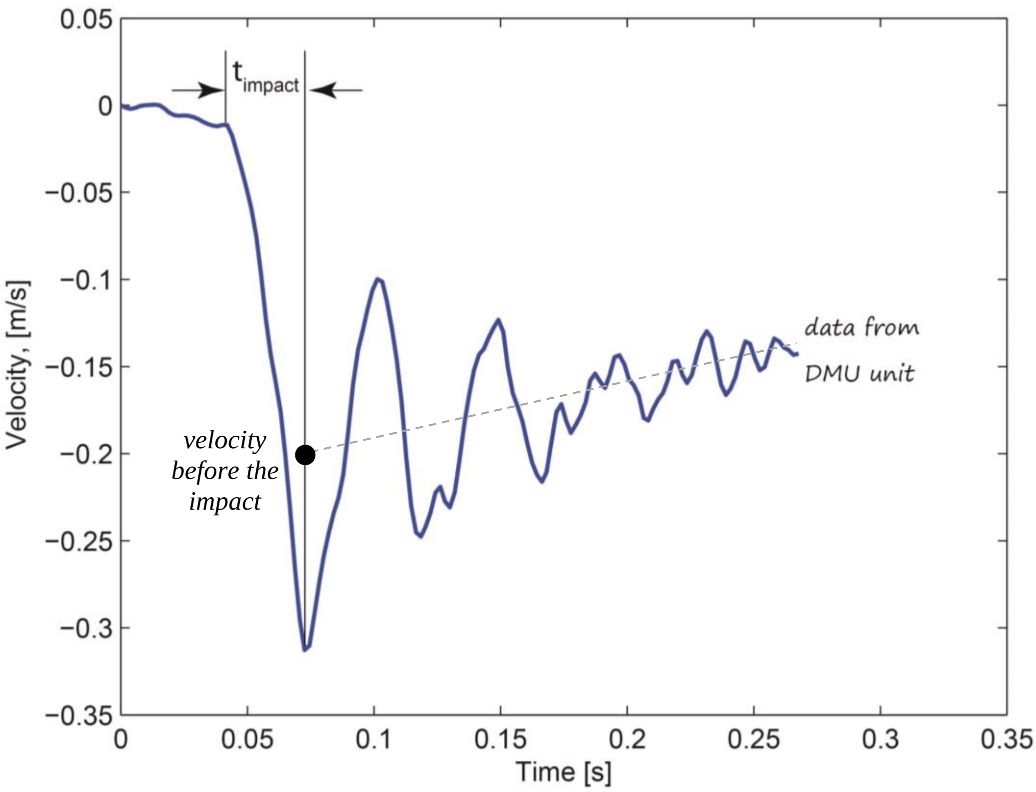


Figure 14: Velocity versus time for Test no. 8; note that the velocity is estimated from the measured acceleration of the floater.

The velocity of the ice block before the collision and the common velocity of the ice block and the floater after the collision were estimated using images extracted from the high-speed video recordings. The procedure for estimation of velocities was the following.

(1) Six frames were obtained from a video sequence (three frames before the impact and three frames after the impact).

(2) Two best visible points were selected: one point – at the top face of the ice block to track the velocity of the ice before impact; another point – at the corner of the floater to track the velocity of the floater before and after impact.

(3) The velocity of the ice block (floater) was found by dividing the distance the corresponding point travelled between two time frames by the time elapsed between

those frames. These results are presented in Table 3. An average of two values is reported in the columns “Velocity before impact” and “Common velocity after impact”.

## 4. Analysis of the main results

The tests were successful and two shared-energy collisions (Test nos. 8 and 9) were achieved in water. During these tests, the ice block failed within the contact area in compressive crushing (Figure 12b) and the structure underwent inelastic deformations (Figure 9). In this section, the main focus will be on the kinetic energy loss in the collision, the severity of structural damage and the maximum impact force.

### *4.1 Collision mechanics*

According to the collision mechanics, the overall loss in kinetic energy at the collision must be absorbed by ice crushing and by deformations of the floater. The principle of conservation of momentum was adopted to determine the common velocity of the ice/floater after a fully-plastic impact (Equation 2) and the demand for strain energy dissipation (Equation 3). The hydrodynamic effects from the surrounding water were treated as added masses.

$$v_c = \frac{(M_i + A_i)v_i + (M_s + A_s)v_s}{M_i + A_i + M_s + A_s} \tag{2}$$

$$E_s = \frac{(M_i + A_i)v_i^2}{2} + \frac{(M_s + A_s)v_s^2}{2} - \frac{(M_i + A_i + M_s + A_s)v_c^2}{2} \tag{3}$$

$v_c$ is the common velocity of the ice/floater after the collision, $E_s$ is the demand for strain energy dissipation, $M_i$ is the ice mass, $M_s$ is the mass of the floater (including the panel), $A_i$ and $A_s$ are the hydrodynamic added masses of the ice and of the floater, respectively and $v_i$ and $v_s$ are the velocities of the ice block and the floater before the impact.

In Equations (2) and (3), for simplicity, the added mass of the ice feature and floater was taken as a constant: $A_i$=0.5$m_i$ (Bass and Sen 1986) and $A_s$=0.4$M_s$ (Petersen and Pedersen 1981). In Equation (3), the common velocity was taken from DMU data. Table 5 presents a comparison between common velocities ($v_c$) predicted by Equation (2) and common velocities estimated from the high speed video (HSV) and DMU data. Also, the table lists the calculated demand for energy dissipation.

Table 5. Common velocity and demand for energy dissipation.

| Test no. | Measured $v_c$, m/s HSV (DMU) | Calculated $v_c$, m/s | Calculated demand for energy dissipation, kJ (%)[a] |
|---|---|---|---|
| 4 | 0.22 (0.09) | 0.12 | 0.64 (93) |
| 8 | 0.40 (0.20) | 0.23 | 2.5 (91) |
| 9 | 0.29 (0.32) | 0.31 | 2.01(77) |
| 11 | 0.20 (0.19) | 0.30[b] | 2.4[b] (92[b]) |

[a] The fraction of dissipated energy versus available kinetic energy; [b] Reduction in the ice-block mass due to melting was neglected.

There is a good agreement between velocities predicted by collision mechanics and the velocity registered by DMU. Differences between velocities from HSV and those calculated indicate that the velocity data from the HSV records are less accurate than those obtained from DMU and are used here for comparison purposes.

The demand for strain energy dissipation was calculated using the velocity data from DMU and is in the range of 0.64–2.4 kJ. The average fraction of dissipated energy versus available kinetic energy is 88%.

### *4.2 Ice-panel interaction in shared-energy regime*

Tests with higher impact energies resulted in larger damage to both the ice and the stiffened panel. A correlation between the ice damage zone and the plastic deformation of the steel panel can be seen in Figure 9. During Test nos. 8 and 9, the local ice behaviour was similar to that in Drop Test no. 1, i.e., the ice block did not split. At the same time, the severity of structural damage in laboratory tests (in water) was less than that in drop tests.

The plate dents in laboratory experiments can be characterized as small dents (in the order of the plate thickness) while the dents in the drop tests are moderate dents. For example, the damage in Figure 11 can be characterized as “hungry horse” and resembles actual ice damages occurring to ships. In Drop Test no. 1, the ratio between the maximum dent-depth (13 mm) and the stiffener spacing (150 mm) is 0.087. This value is close to that calculated using full-scale damage values and scantlings reported in Hänninen (2005), i.e., permanent dents on the plating of a chemical tanker caused by a collision with multi-year ice. Both ratios (0.087 – from the experiment and 0.086 – from full-scale) are larger than existing criteria for in-service allowance of hull plating, i.e., a ratio of 0.05 (Jennings et al. 1991), and larger than two times the plate thickness.

### *4.2.1 Plastic limit analysis*

It is of interest to perform analytical comparisons to the experimental results. A simplified theoretical model was applied to the experimental data (Test no.8 and 9) to back calculate the maximum impact load from the known permanent deformations. The analytical model is based on plastic mechanisms analysis, measured plate deflections and the ice damage zone. Any effects of membrane stresses were neglected. The yield stress of the panel elements was taken from Table 1. To account for strain-rate effects the dynamic yield stress ($\sigma_{Yd}$) was estimated in accordance with the Cowper-Symonds equation (Cowper and Symonds 1957) where coefficients $c$=40, $q$=5 and the strain rate is 1.0 $s^{-1}$.

In Test no. 8, the plate deformations are very local. The impact load was estimated as a sum of the critical load from a yield-line model (square plate, clamped boundaries) and the load from an end-loaded stiffener model (Figure 15). The end-loaded stiffener model was similar to the Daley's (2002) expression. Our model differed from the Daley's model in that the plastic work done by the plastic bending moments in the left part of the beam was neglected. The location of the plastic hinge in the presented model (Figure 15) was based on the actual plate deflections, whereas Daley (2002) determined the location of the hinge by minimizing the internal work. Furthermore, the end-loaded stiffener model included also a concentrated load at a distance of approximately 0.1 m from the right end. The latter was done because we observed (from Figure 9) that 25% of the critical load (calculated with the yield-line model) could be carried by the stiffener; see deformation pattern for Test no. 8, load patch $b^*$.

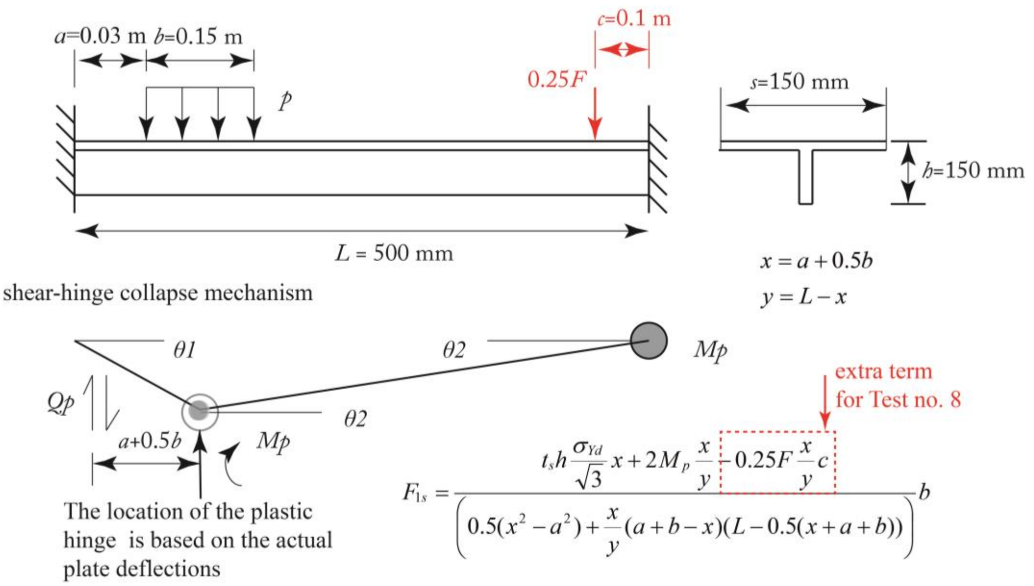


Figure 15. Fully clamped stiffener model with the assumed plastic mechanism ($L$ – frame spacing; $M_p$ – plastic bending moment of T cross-section; $p$ – pressure; $\theta_1$ and $\theta_1$

– rotation angles of the beam; $Q_p$ – shear force; $h$ – stiffener height; $t_s$ – stiffener thickness; $s$ – stiffener spacing; and $F_{1s}$ – collapse load for one stiffener).

For Test no. 9, the impact load was calculated using the "*end loaded fixed-fixed frame model*" formulated by Daley (2002). The results of the calculations are presented in Table 6.

Table 6. Summary of analytical calculations.

| Test no. | Calculated force, kN | Measured force (DMU estimates), kN |
|---|---|---|
| 8 | 117 | 190 |
| 9 | 162[a] | 203 |

[a] the value corresponds to the collapse of two stiffeners;

Data in Table 6 indicate that forces predicted by the analytical calculations are lower than the measured impact forces (DMU empirical estimates). Additional analysis of roll rate data revealed that accounting for the roll rate in the calculations of the impact forces can influence the DMU estimates by approximately 5–10%. Consequently the gap between the calculated and measured forces could be smaller than that in Table 6, and it can be argued that the analytical calculations support the measurements. Moreover, the Daley's end-loaded fixed-fixed frame model for the collapse of two stiffeners provides a good estimate of the maximum impact force for Test no. 9.

To summarize, the simplified theoretical model were applied to the experimental data to back calculate the maximum impact load from the known permanent deformations. The analytical calculations support the measurements, and the good estimate of the force is given by Daley's end-loaded fixed-fixed frame model for the collapse of two stiffeners.

#### 4.2.2 *Numerical simulations*

A finite element analysis was carried out to investigate the shared-energy regime and the energy dissipation in the structure and ice. Test no. 9 was selected as it showed the largest extent of damage to the stiffened panel. Further, the indentation measured in Test no. 9 suggests a large contact area of fairly symmetric proportions (see Figure 9). As the exact ice geometry was not recorded at impact, a spherical ice contact was assumed for the simulation (Figure 16). The numerical procedure will be explained first, followed by the results of the simulations.

The explicit non-linear finite element software LS-DYNA R6.1.0 was used. The steel behaviour was modelled as an elasto-plastic material with a constant tangent hardening modulus, which is a good approximation based on the uniaxial tensile test of the struck plate as reported in Kim et al. (2013). Strain-rate effects were accounted for by assuming a visco-plastic Cowper-Symonds hardening with strain-rate parameters $C$=40 and $q$=5 as recommended by Cowper and Symonds (1957) for mild steels. The ice behaviour was modelled using the elliptic yield criterion and the strain–based pressure dependent failure criterion for granular freshwater ice as proposed by Liu et al. (2011). The parameters for the ice model was determined using an empirical pressure-area relation ($p$=0.35$A^{-0.5}$) , which is determined using a lower bound estimate of indentation tests on freshwater granular ice within the brittle regime (Kim et al. 2012b). The pressure-area relation takes into account effects of ice temperature and microstructural characteristics. The parameters that were used for the analysis are listed in Table 7.

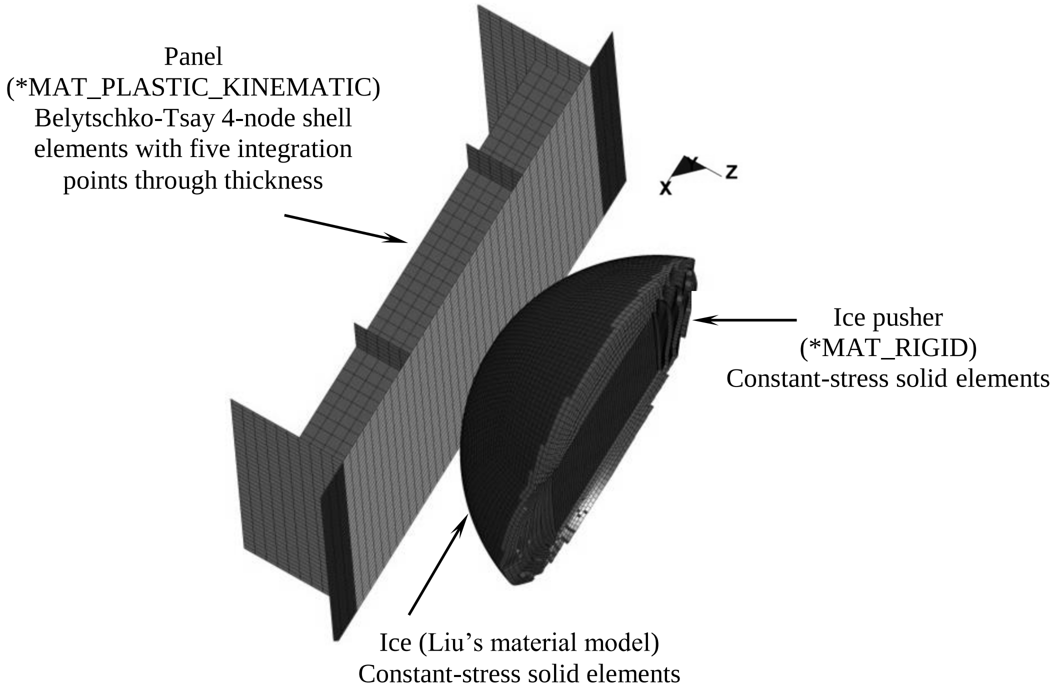


Figure 16. Finite element model of the stiffened panel and the simplified geometry of the ice block for Test no. 9.

The ice was meshed with an average element size of 15 mm, and the stiffened panel with mesh size of 30 mm. The stiffened panel is assumed to be stationary during the impact, whereas the ice is given an initial velocity and kinetic energy corresponding to the experiment. Validation of the numerical model was done by comparing experimental results of Test no. 9 with the results of numerical simulation.

Table 7. Material parameters used in numerical simulations.

| **Ice parameters for Liu's model** | **Value** | **Steel parameters** | **Value** |
|---|---|---|---|
| Ice block radius, (m) | 0.45 | Young's modulus, (GPa) | 210 |
| Ice density, (kg/m3) | 900[a] | Initial yield stress (MPa), 2mm plate | 190 |
| Young's modulus, (GPa) | 9.5[a] | Initial yield stress (MPa), 4mm plate | 360 |
| Poisson ratio, (-) | 0.3[a] | Hardening modulus (MPa) | 1422 |
| Inelastic $a_0$, (MPa$^2$) | 2.588[a] | Cowper-Symonds, $C$ | 40 |
| Inelastic $a_1$, (MPa) | 8.630[a] | Cowper-Symonds, $q$ | 5 |
| Inelastic $a_2$, (-) | 0.163[a] | | |
| Initial failure strain, (-) | 0.01[a] | | |
| Ice-steel friction (-) | 0.15 | | |

[a] Ice parameters correspond to the empirical pressure-area relationship obtained from indentation of freshwater ice.

Figure 17a shows the calculated impact force and the DMU force in Test no. 9. Figure 17b shows the permanent plastic deformation of the panel after impact. This resulting deformation of the stiffened panel can be compared to the experimentally observed damage in Figure 9. Figure 17c shows a comparison between the calculated plate deflection profile and the measured values.

A

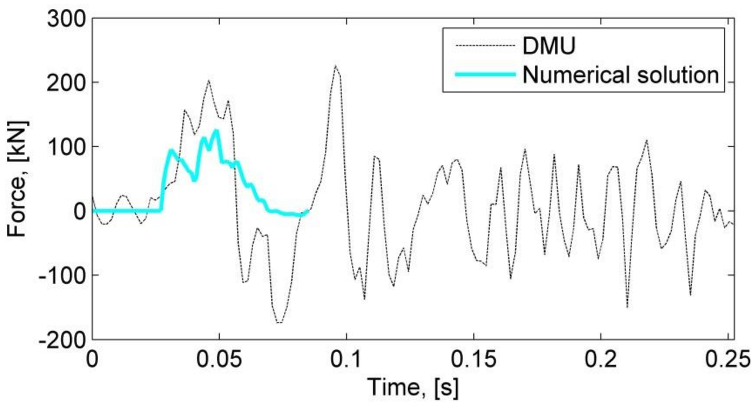


(a)

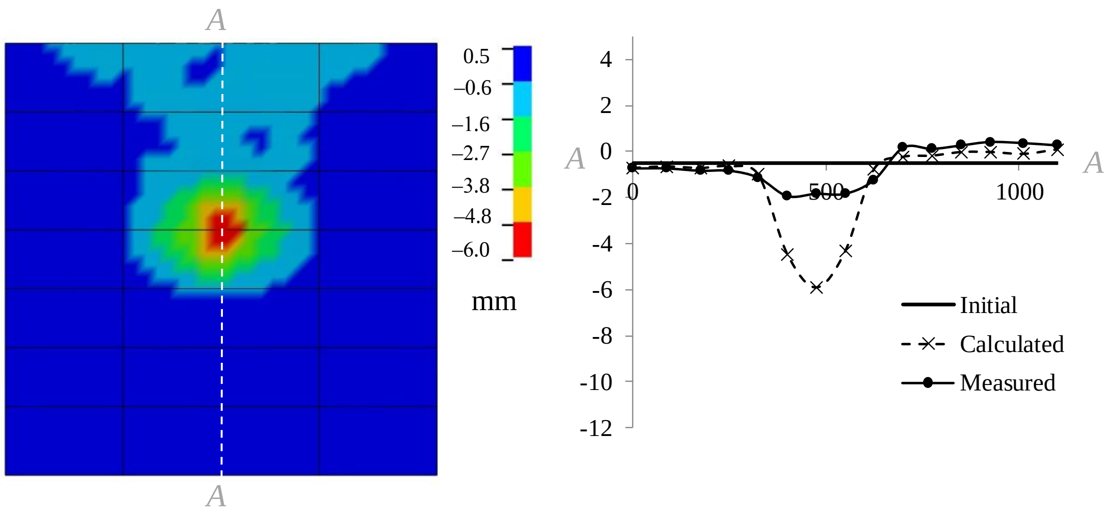


(b) (c)

Figure 17. Results of the numerical simulation: (a) impact force; (b) displacement contour (units: mm) of the plate after impact; the black horizontal and vertical lines indicate the locations of the stiffeners and the frames; (c) plate deflection profile (A-A), (units: mm).

The peak force in the simulation was 126 kN (Figure 17a), compared to the 203 kN in the experiment and to the 162 kN in analytical calculations (plastic limit analysis in Section 4.2.1). From the simulations, the plastic energy dissipation that is required to cause the structural damage is 0.68 kJ, (28 %) of the total available kinetic energy. The external mechanics calculation estimated 2.01 kJ to be dissipated in total, thus leaving 1.33 kJ for ice crushing. From the simulation, the dissipated energy in the ice is 1.70 kJ; that is 28% more than in the experiment. This difference is acceptable because 1) the boundary conditions for the finite element model were an idealised version of the physical conditions (i.e., water supporting the plate and the bolted connections were not modelled) and 2) there are uncertainties in the actual ice-structure contact interface. In future, the numerical simulations will be carried out considering the surrounding water.

Overall, a satisfactory agreement between the simulations and measurements verifies the competence of the analysis as well as the ice model.

The present model is able to capture the shared-energy interaction between the ice-block and the stiffened panel. The calculations show that panel dissipated 28 % of the available kinetic energy. This energy dissipation in the panel is likely overestimated, because as indicated in Figure 17c, the actual inelastic deformations of the stiffened panel were less pronounced than those in the simulation. Thus, the amount of the dissipated energy in the plate would be less than the calculated 0.68 kJ.

The results turned to be very sensitive to the ice input data. The numerical simulations with small differences in the ice failure parameters highlighted that the transition between a near rigid ice response and progressive crushing failure is very narrow. Small changes in the ice input data may significantly change the outcome in terms of structural deformations and energy dissipation. This finding of high sensitivity to relative strength is similar to that for ship-ship collisions as in Storheim and Amdahl (2014).

In summary, the results demonstrate that under laboratory conditions, it is possible to achieve collisions within the shared-energy deformation regime with small to moderate damage on the stiffened panels (see Test nos. 8, 9 and Drop Tests). During collision, both the ice and the structure have dissipated energy through inelastic deformation. A good agreement between the numerical simulations, the experimental results and analytical calculations was achieved. The ice material model proposed by Liu et al. (2011) and the numerical procedure as a whole were able to predict the history of first impact and plate deformations with reasonable accuracy. The exact level of damage to the panel and the maximum impact force were difficult to predict with the model, but the calculated deflections and the maximum force are of the same order of magnitude.

## 6. Discussion

In attempting to model the shared-energy ice-structure collision, the ice block was towed to impact the structure. The results of collision tests and numerical simulations have been presented, where both the ice and the structure underwent inelastic deformations during the collision, but due to safety considerations, the degree of energy dissipation was less than the initial aim of the tests. The structural deformations were limited to small (or moderate) dents on the impacted panels. Before these laboratory tests were carried out, hardly any experience existed on how to conduct shared-energy collision tests successfully. The data presented in this paper demonstrate that under laboratory conditions it is possible to achieve a shared-energy interaction between freshwater ice blocks and the steel floating structure. These results and their applicability will be discussed in the following paragraphs. Furthermore, lessons learned from the laboratory test campaign will be presented.

The setup could to some extent represent a wave/current-induced impact of an ice block onto a stationary object. This was the first experiment of its kind; the experimental apparatus has balanced the accuracy of the results with the total costs. One may argue that the chosen collision scenario is unrealistic in the sense that the ice block is being dragged through the water to impact a stationary structure. The choice of the collision scenario (and the experimental apparatus) was limited due to safety restrictions of the ice basin, namely the maximum speed allowed by the towing carriage and the strength of the concrete floor and the walls of the ice basin. Towing a 7.5-tonne structure was nearly impossible under laboratory conditions.

The use of weak model ice in scenarios where ice fails in compression is debated (Jordaan et al. 2012). In the reported experiments, no scaling by similitude laws was applied. The ice was produced based on laboratory experiences to replicate the behaviour of freshwater granular ice at impact. The resulting ice was predominantly granular. This was a desirable outcome because the mechanical behaviour of granular ice is known to be similar to that of glacier ice (Montgnat et al. 2009). Observations of the ice microstructure (Section 2.2.2) indicate that the laboratory-grown ice exhibits few similar characteristics as iceberg ice (i.e., presence of air bubbles of different sizes, healed cracks), but at the same time, the shape of the grains, the character of air bubble accumulation and the amount of grain interlocking are different from those in iceberg ice; see, e.g., data in Gagnon and Gammon (1995) and Barrette and Jordaan (2001). The laboratory-grown ice had rounded grains, while iceberg grains are generally irregular in shape. It is not certain how these differences affect mechanisms of the ice-structure interaction. In fact, visual observations of ice damage in the laboratory (Figure 12) are very similar to those reported in the field (Jordaan 2001). Moreover, the measured values of ice strength under uniaxial loading are similar to the values reported in Michel (1978) for polycrystalline ice at 0°C within the brittle regime. Similar to the behaviour of growlers (see Gagnon 2004), the laboratory-grown ice blocks appear to be resistant to impacts. An ice block could withstand many impacts without significant damage to bulk ice under prescribed impact conditions (i.e., only local damage to the impacted ice corner). In summary, the compressive behaviour of the laboratory-grown ice resembles that of freshwater granular ice and to a certain extent, iceberg ice.

From Figure 9 it can be seen that the ice damage zone was highly localized in Test nos. 8, 9 and Drop Test no. 1; and it may be argued that the presence of healed cracks in ice samples (e.g., see Figure 12b) did not significantly affect the response of the ice. In

Drop Test no. 2, any presence of healed cracks attributed to shattering of the ice block. Tables 3 and 4 show that the ice crushing failure mode has dominated in tests with lower impact energies, whereas it was opposite for higher impact energies – the splitting failure mode has dominated. A possible reason for the ice blocks to fail in either mode is the ratio between the kinetic energy immediately before the impact and the size of the ice block. Data in Table 4 indicate that with the ratio of < 3.5 kJ/0.9 m, the localized ice crushing dominated, whereas the ratio of ~17.7 kJ/0.9 m led to the splitting-dominated failure mode and to the completely shattered ice block.

The character of force-histories (Figure 13) is similar to those in Bruneau et al. (1994) for iceberg impacts and includes the impact and the damped dynamic response of the panel. The primary hit and the maximum loads have been emphasized in this paper. The laboratory test results and their analysis in Section 4.2.1 showed that the peak force estimated from DMU measurements can be back-calculated using the measured plate deflections and observations of the ice damage zone. In addition, the peak force from numerical simulations (Section 4.2.2) is in the same range with back-calculated peak force and also with that from DMU. There is a good agreement between theory, numerical simulations and the experimental results, which increase the confidence in the derived experimental impact force. A direct force measurement would have been preferable.

The results of numerical simulations indicate that the ice block dissipated the major part of the available kinetic energy. This finding is similar to that in Kim et al. (2013) for drop ice tests on stiffened panels.

The numerical simulation of only one shared-energy test (Test no. 9) was performed by simplifying geometry of the ice-block into a sphere instead of the truncated prism. In Test no. 8, the character of plate deflections suggests that the local ice shape at contact was rather a wedge. At this juncture, in order to simulate Test no. 8, an additional assumption about the local ice shape needs to be made. Therefore, it is premature to go further than we have. Our sense, however, is that given the actual local ice shape for the Test no. 8, the numerical simulations will predict the maximum impact force and panel deformations with a reasonable degree of accuracy.

## 7. Conclusions

Laboratory tests of impact between freshwater ice blocks and deformable steel panels were successfully performed. This was a new attempt to model shared-energy ice-structure collisions in water and the results of this study are important for designing experiments on structural deformation (damage) from ice actions.

Two shared-energy collisions were achieved in water (i.e., the ice block fails within the contact area in compressive crushing and the structure undergoes inelastic deformations). Analytical back calculations of the impact forces and numerical simulations were performed to support the findings of these tests. The major findings are the following:

- The behaviour of laboratory-grown ice resembled that of freshwater granular ice.
- The structural deformations were limited to small (or moderate) dents on the impacted panels.
- The impacts of ice blocks at speeds of 1–2 m/s with panels of different stiffness produced various results, ranging from (3–5)-mm dents in 2 mm- and 4 mm-thick plates to no visible marks (on a 12 mm-thick plate).
- Drop tests on the same panels with higher impact energies resulted in larger damage to both the ice and the stiffened panel. The ratio between

the maximum dent-depth and the stiffener spacing was 0.087, which is larger than the maximum allowable in-service plate-deformation ratio of 0.05 for vessels.

- A good agreement between theory, numerical simulations and the experimental results was achieved. The Daley's end-loaded fixed-fixed frame model for the collapse of two stiffeners provided the good estimates of maximum impact forces in shared-energy tests.
- The results of numerical simulations were found to be very sensitive to the ice input data. The transition between near rigid ice response and progressive failure was found to be very narrow.
- The ice material model proposed by Liu et al. (2011) and the numerical procedure were able to predict the character of the force-time history and structural deformation with reasonably good accuracy but underestimated the maximum force.

Lessons-learned from the execution of the impact tests in water are summarized below.

- *Ice specimen preparation*: For future experiments, a unidirectional freezing process is recommended. This can be done by isolating the sides and top of the ice moulds.
- *Geometry of ice specimen*: Alternative ways to control the ice-shaping process and to collect data on its shape should be considered, e.g., a band saw with a tilting worktop and a 3D-scanning device. Furthermore, the size of the ice block is also an important parameter. To avoid splitting-dominated ice failure, the usage of larger (or confined) ice blocks and lower impact velocities is preferred.

- *Controlling direction of impact and kinetic energy*: Feasibility of quasi-static and dynamic tests in dry conditions versus dynamic tests in water should be checked.
- *Instrumentation*: A direct measurement of loads (i.e., load cells) is preferred over indirect methods (e.g., by recording accelerations and strains). A pressure sensing device should be chosen such that it is able to respond to a rapid variation in pressures and the calibration of the device is manageable for a wide range of pressures (0–100 MPa). In dry conditions, one can directly record (and observe) amount of crushed ice by simply collecting it, while in water, weighing of the ice block before and after the impact may be performed, assuming the amount of crushed ice is sufficiently large to be recorded accurately.

The results of the present study provide an example of modelling of shared-energy collisions in the laboratory, and may be used to support the development of the testing procedure for a full-scale ice-structure shared-energy collision scenario. A successful application of the presented results and the lessons-learned is a pilot study of ice-structure collisions in a pendulum accelerator by Storheim et al. (2015).

**Acknowledgements**

The work described in this publication was supported by the Seventh Framework Programme of the European Community through a budgetary fund to the Integrating Activity HYDRALAB IV FP7, Contract no. 261520 and funding from the Sustainable Arctic Marine and Coastal Technology Centre (SAMCoT, WP4), Project no. 203471. The authors gratefully acknowledge Prof. Sören Ehlers and Prof. Mauri Määttänen for their helpful comments during experimental design. We especially thank to Keijo

Hanhirova, Panu Sainio, Pentti Tukia, Juha Alasoini and to Teemu Rintapäivä for their comments and invaluable technical assistance in conducting the experiments and in post-processing results. The authors would like to thank Prof. Jukka Tuhkuri and Dr. Dan Masterson for providing valuable hints about earlier shared-energy experiments.

## References

Alsos, H.S. and Amdahl, J., 2009. On the resistance to penetration of stiffened plates, Part I – Experiments. International Journal of Impact Engineering, 36 (6), 799–807.

Barrette, P.D. and Jordaan I.J., 2001. Beam bending and fracture behaviour of iceberg ice. PRED/CHC report 4-78, Ocean Engineering Research Canter, Memorial University of Newfoundland.

Bass, D. & Sen, D., 1986. Added mass and damping coefficient for certain "realistic" iceberg models. Cold Regions Science and Technology 12 (2), 163–174.

Bruneau, S.E., Cammaert, A.B. and Croasdale, K.R., 1994. Field tests for iceberg impact loading. Proceedings of the 12th International Symposium on Ice 1, 187–197.

Cowper, G. R. and Symonds, P. S., 1957. Strain-hardening and strain-rate effects in the impact loading of cantilever beams. Technical report no. 28, Brown University, Division of Applied Mathematics.

Daley, C.G., 2002. Derivation of plastic framing requirements for polar ships. Marine Structures 15 (6), 543–559.

Daley, C.G., Phillips, L.D. and McCallum, J.S., 1986. Dynamic Ship/Ice Impact – Results of Parametric Model Testing. Proceedings of Ice Technology Conference.

Duthinh, D., Engler, M., Klein, K. and Regrettier, J.-F., 1990. Full scale iceberg impact: a pilot experiment in Antarctica. Proceedings of the 10th International Symposium on Ice 2, 890–901.

Gagnon, R.E. and Gammon, P.H., 1995. Characterization and flexural strength of iceberg and glacier ice. Journal of Glaciology 41(137), 103–111.

Gagnon, R.E, 2008. Analysis of data from bergy bit impacts using a novel hull-mounted external Impact Panel. Cold Regions Science and Technology 52(1), 50–66.

Gagnon, R.E., 2004. Analysis of laboratory growler impact tests. Cold Regions Science and Technology 39 (1), 1–17.

German and Milne/VTT, 1985. M.V. Arctic test results and analysis, Final Report to Transport Canada, Coast Guard Northern Report No. TP6270 E.

Ghoneim, G.A.M. and Keinonen, A.J., 1983. Full-scale impact tests of CANMAR Kigoriak in thick ice. Proceedings of the 7th International Conference on Port and Ocean Engineering Under Arctic Conditions, 3, 329–346.

Hänninen, S., 2005. Incidents and accidents in winter navigation in the Baltic Sea, winter 2002 – 2003. Technical Report Winter Navigation Research Board, Helsinki. Research Report no. 54.

Hill, B., 2005. Ship collisions with iceberg database, Report to PERD: Trends and analysis, TR-2005-17.

IACS' Unified requirements, 2011. Requirements concerning Polar Class, The International Association of Classification Societies (IACS)

Jennings, E., Grubbs, K., Zanis, C. and Raymond, L., 1991. SSC–364 inelastic deformation of plate panels. Technical report SR-1322, Ship Structure Committee.

Jordaan, I., Taylor, R. and Derradji-Aouat, A., 2012. Scaling of flexural and compressive ice failure. Proceedings of the 31st International Conference on Ocean, Offshore and Arctic Engineering. Rio de Janeiro, Brazil, Paper OMAE2012-84033.

Jordaan, I.J., 2001. Mechanics of ice structure interaction. Engineering fracture mechanics 68 (17-18), 1923–1960.

Kim, E. and Amdahl, J., 2013. Review of existing methods for the analysis of the accidental limit state due to ice actions. Proceedings of 6th International Conference on Collision and Grounding of Ships and Offshore Structures, 221–231.

Kim, E., Golding, N, Schulson, E.M., Løset, S. and Renshaw, C.E., 2012a. Mechanisms governing failure of ice beneath a spherically-shaped indenter. Cold Regions Science and Technology 78, 46–63.

Kim, E., Storheim, M., Amdahl, J., Løset, S. and von Bock und Polach, R., 2013. Drop tests of ice blocks on stiffened panels with different structural flexibility. Proceedings of 6th International Conference on Collision and Grounding of Ships and Offshore Structures, 241–250.

Kim, E., Storheim, M., von Bock und Polach, R. and Amdahl, J., 2012b. Design and modelling of accidental ship collisions with ice masses at laboratory scale. Proceedings of the 31st International Conference on Ocean, Offshore and Arctic Engineering 6, 495-506.

Lindholm, J.E., Riska, K. and Joensuu, A., 1990. Contact between structure and ice: Results from ice crushing tests with flexible indentor. Report M-101, Helsinki University of Technology, Espoo.

Manuel, M., Gudimetla, P.S.R., Daley, C. and Colbourne, B., 2013. Controlled plastic deformation of a grillage using artificial freshwater ice at large scale. Proceedings of the 22nd International Conference on Port and Ocean Engineering under Arctic Conditions, Espoo, Finland, Paper POAC13_157.

Masterson D.M., Frederking, R.M.W., Jordaan, I.J. and Spencer P.A., 1993. Description of multi-year ice indentation tests at Hobson's Choice Ice Island – 1990. Proceedings of 3rd International Conference on Ocean, Offshore and Arctic Engineering 4, 145–155.

Michel, B., 1978. Ice mechanics. Les Presses De L’Université Laval, Qubéc, 499p.

Montagnat, M., Durand, G. and Duval, P., 2009. Recrystallization processes in granular ice. Supplement Issue of Low Temperature Science 68, 81–90.

NORSOK STANDARD N-004, 2013. Design of steel structures. Standard, Norway.

Petersen, M.J. and Pedersen, T., 1981. Collisions between ships and offshore platforms. Proceedings of the Offshore Technology Conference, 163–172.

Popov, Y.N. Faddeev, O.N. Kheisin, D.E. and Yakovlev, A.A., 1967. Strength of ships navigating in ice. Sudostroenie Publ. House: Leningrad, (in Russian).

Ritch, R., Frederking, R., Johnston, M., Browne, R. and Ralph, F., 2008. Local ice pressures measured on a strain gauge panel during the CCGS Terry Fox bergy bit impact study. Cold Regions Science and Technology 52 (1), 29–49.

Snider, D., 2012. Polar ships operations – a practical guide, The Nautical Institute, 136p.

Storheim, M., Nord, T., Kim, E., Høyland, K., Langseth, M., Amdahl, J. and Løset, S., 2015. Pilot study of the ice-structure interaction in a pendulum accelerator. Proceedings of the 23rd International Conference on Port and Ocean Engineering under Arctic Conditions, Paper 213.

Tuhkuri, J., 1993. Laboratory tests of ship structures under ice loading, 1–3, Otanemi M-166.

Varsta, P. and Riska, K., 1982. Measurement of ice pressures and forces on Canmar Kigoriak during repeated trials in 1981. Report LAI-332/82, Technical Research Centre of Finland, Dome Petroleum Limited.